iScience

CellPress
OPEN ACCESS

Article

Water-dispersible Ti3C2Tz MXene nanosheets by molten salt etching

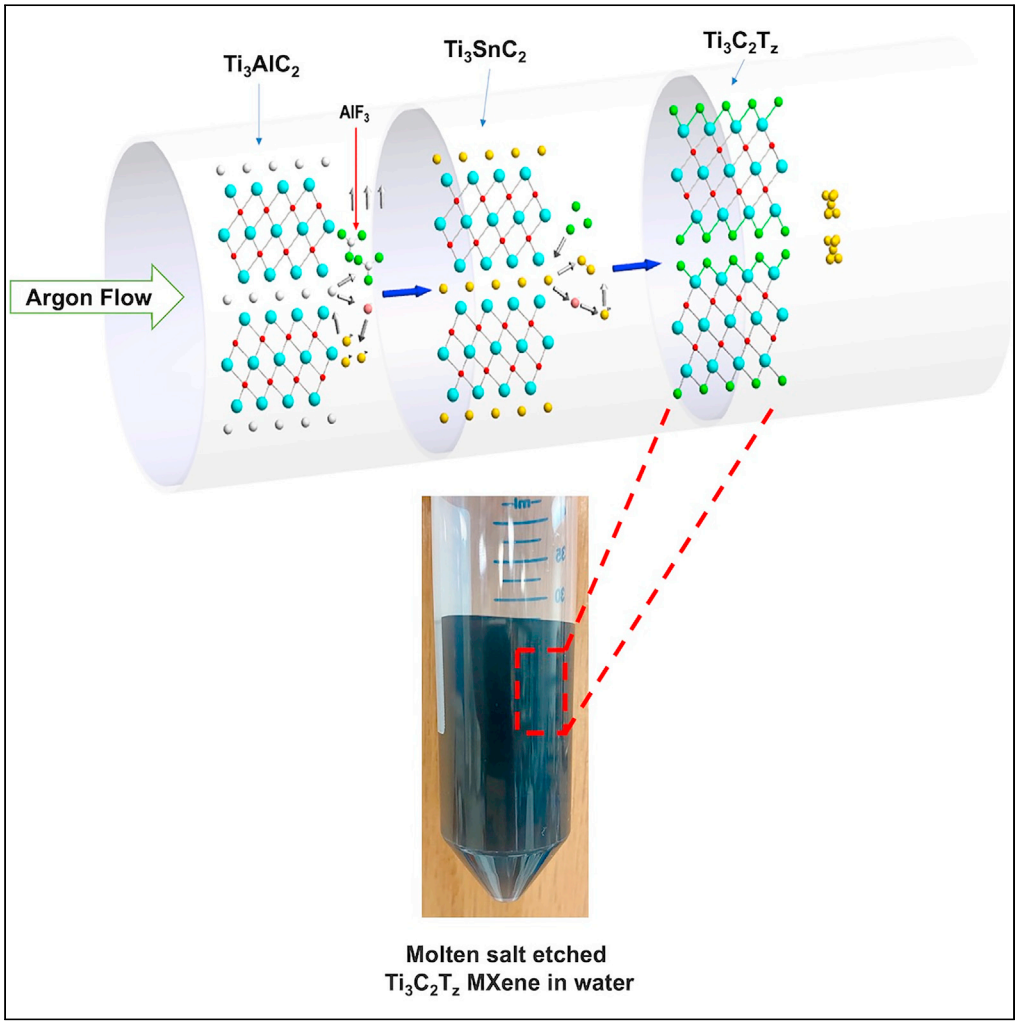

Kailash Arole, Jackson W. Blivin, Sanjit Saha, ..., Miladin Radovic, Jodie L. Lutkenhaus, Micah J. Green

micah.green@tamu.edu

Highlights

Nonhazardous route of MXene synthesis

Industrially scalable process for the MXene production

Arole et al., iScience *24*, 103403
December 17, 2021
https://doi.org/10.1016/j.isci.2021.103403

iScience

CellPress
OPEN ACCESS

Article

Water-dispersible Ti3C2Tz MXene nanosheets by molten salt etching

Kailash Arole,[1] Jackson W. Blivin,[2] Sanjit Saha,[2] Dustin E. Holta,[1] Xiaofei Zhao,[2] Anubhav Sarmah,[2] Huaixuan Cao,[2] Miladin Radovic,[1] Jodie L. Lutkenhaus,[1,2] and Micah J. Green[1,2,3,*]

SUMMARY

Molten-salt etching of Ti_3AlC_2 MAX phase offers a promising route to produce 2D $Ti_3C_2T_z$ (MXene) nanosheets without hazardous HF. However, molten-salt etching results in MXene clays that are not water dispersible, thus preventing further processing. This occurs because molten-salt etching results in a lack of -OH terminal groups rendering the MXene clay hydrophobic. Here, we demonstrate a method that produces water-dispersible $Ti_3C_2T_z$ nanosheets using molten salt (SnF_2) to etch. In molten salt etching, SnF_2 diffuses between the layers to form AlF_3 and Sn as byproducts, separating the layers. The stable, aqueous $Ti_3C_2T_z$ dispersion yields a ζ potential of −31.7 mV, because of -OH terminal groups introduced by KOH washing. X-ray diffraction and electron microscopy confirm the formation of $Ti_3C_2T_z$ etched clay with substantial d-spacing as compared with clay etched with HF. This work is the first to use molten salt etching to successfully prepare colloidally stable aqueous dispersions of $Ti_3C_2T_z$ nanosheets.

INTRODUCTION

In recent years, 2D nanosheets referred to as "MXenes" have caught the world's attention because of their wide compositional range and remarkable set of properties as well as processability in water for inks and coatings (Barsoum, 2000; Eklund et al., 2010, 2017; Naguib et al., 2011, 2012, 2014b; Tezel et al., 2022). MXenes are prepared by the selective etching of the A-layer element from a parent $M_{n+1}AX_n$ (or MAX) phase, where M is an early transition metal (Ti, V, Nb), A is an element from groups 13–16, and X is carbon or nitrogen. The general formula for MXenes is $M_{n+1}X_nT_z$ (n = 1–3), where T_z stands for the surface terminations, such as -F, -Cl, -OH, or -O, which are bonded to outer M layers on 2D nanosheets (Shah et al., 2017; Seh et al., 2016). Because of their material properties, such as metallic conductivity and hydrophilicity, MXenes have been used in wide range of applications in energy storage, catalysis, electromagnetic interference shielding, surfactant, sensor, composites, and batteries (Khazaei et al., 2017; Ran et al., 2017; Li et al., 2018; Tang et al., 2012; Shahzad et al., 2016; Ghidiu et al., 2014a; Persson et al., 2019; Kim et al., 2018; Cao et al., 2021).

Since the synthesis of $Ti_3C_2T_z$ in 2011, MXenes have been generally prepared by the selective etching of the A-layer in an aqueous solution containing fluoride ions such as aqueous hydrofluoric acid (HF). Other methods include the use of a mixture of hydrochloric acid (HCl) and fluoride salts (such as LiF) or ammonium bifluoride $(NH_4)HF_2$ (Feng et al., 2017; Naguib et al., 2011). The significant drawbacks of HF-related methods are the inherent dangers of using HF, its waste management, scalability, and lack of versatility in etching MAX phase (Lakhe et al., 2019).

In order to overcome the dangers and challenges of the HF-related etching techniques, a new MXene synthesis method has been developed, which uses molten salt as the etchant (Kamysbayev et al., 2020; Li et al., 2019, 2020; Urbankowski et al., 2016). The molten salt method is less hazardous than traditional methods because HF is not involved. In addition, this reaction is completely contained during the etching process and requires little intervention or exposure to the chemicals, which is not the case with HF-related methods. However, this method has not yet produced MXenes that could be dispersed in water, thus preventing easy processing in water-based inks, coatings, and sprays.

In 2016, Urbankowski et al. first reported the use of molten salts to create nitride MXenes by etching parent MAX phase in a eutectic mixture of fluoride salts (Urbankowski et al., 2016). Later, Li et al. synthesized

[1]Department of Materials Science and Engineering, Texas A&M University, College Station, TX 77843, USA

[2]Artie McFerrin Department of Chemical Engineering, Texas A&M University, College Station, TX 77843, USA

[3]Lead contact

*Correspondence: micah.green@tamu.edu

https://doi.org/10.1016/j.isci.2021.103403

$Ti_3C_2T_z$ MXene with an element replacement approach, where Al in MAX phase is first replaced by Zn, followed by the removal of Zn; to do so, they performed a reaction between Ti_3AlC_2 with $ZnCl_2$, a Lewis acid, at 550°C (Li et al., 2019). The final product is a Cl-terminated $Ti_3C_2T_z$ clay with typical accordion structure, but no water dispersible and separated nanosheets were reported. In 2020, Li et al. used redox-controlled A-site etching in Lewis acid molten salts to synthesize MXenes from several MAX phase precursors with Si, Zn, and Ga as the A element. In that work, they mixed the MAX phase powder with a combination of salts such as $CuCl_2$, NaCl, and KCl and heated the mixture to 750°C for 24 h inside an alumina tube under flowing argon (Li et al., 2020). They were able to create $Ti_3C_2T_z$ clay, but they were unable to delaminate it into single-layer nanosheets as the previous paper. Kamysbayev et al. reported the ability to tailor the surface groups of MXenes using $CdBr_2$ and $CdCl_2$ molten salts and are also the only group to date to go beyond etched MXene "clays" and produce dispersed $Ti_3C_2T_z$ nanosheets (Kamysbayev et al., 2020) but in N-methylformamide (NMF), not in water. They also found that after the initial etching of the MAX phase, the MXene terminal groups predominantly contain the halogen group of the salt. With a secondary molten salt treatment, the authors were able to exchange the terminal groups. The molten salt method of etching is promising for its versatility in the wide variety of etchable MAX phases and its ability to select the terminal groups of the MXene.

In the following work, we develop the first-ever molten-salt method to create colloidally stable $Ti_3C_2T_z$ nanosheets in aqueous solution. This is the first reported use of SnF_2 as the etchant to form fluorine-terminated $Ti_3C_2T_z$ nanosheets. Using SnF_2 as the etchant produces an extremely open $Ti_3C_2T_z$ clay structure. A KOH wash of the clay was necessary for the addition of hydrophilic -OH groups on MXene that promoted the formation of a stable aqueous dispersion.

RESULTS AND DISCUSSION

The molten salt etching procedure was carried out as follows: a mixture of Ti_3AlC_2 and Tin fluoride (SnF_2) was heated for 6 h (Figure 1), resulting in the formation of $Ti_3C_2T_z$ clay with some Sn spheres. After etching, the $Ti_3C_2T_z$ clay was washed with potassium hydroxide (KOH) solution to dissolve and remove the excess or unreacted SnF_2 crystals. KOH-washed $Ti_3C_2T_z$ clay was intercalated with dimethyl sulfoxide (DMSO) and then washed with water to remove DMSO. After intercalation, the $Ti_3C_2T_z$ clay was delaminated by bath sonication, and the dispersion of delaminated $Ti_3C_2T_z$ is centrifuged; this resulted in a stable dispersion of $Ti_3C_2T_z$ nanosheets. The processing schematic is shown in Figure S1.

A fluoride salt was desired for molten salt etching due to fluorine's higher electronegativity relative to chlorine. A higher electronegativity was desired to aid in etching the A-layer in MAX phase especially for those that Li et al. showed could not be etched by chloride salts (Li et al., 2019). For the molten salt to be composed of a single salt, the melting point needed to be less than 800°C (the temperature at which MXene begins to degrade). Tin(II) fluoride has a melting point of 213°C and is one of the few fluoride salts with a melting point below the required temperature. Sn has the additional advantage of having a large atomic radius of 158 pm, which may improve interlayer spacing in the MXene clay based on the reaction mechanism proposed by Li et al. In addition to this, the intermediate phase (Ti_3SnC_2) formed during the etching is a thermodynamically stable phase that aids the further process and gives the $Ti_3C_2T_z$ MXene. The other advantage of using SnF_2 over liquid mixture of HCl and LiF is that solid SnF_2 provides the safer way of handling over any liquid hazardous chemicals.

After heating the mixture of Ti_3AlC_2 and SnF_2 with a mole ratio of 1:6 at 550°C for 6 h, a $Ti_3C_2T_z$ clay was formed, along with Sn spheres present. The SEM images (Figure 2B) show the typical "accordion" structure of $Ti_3C_2T_z$ clay, indicating successful etching of the A element, with clear expansion between the basal planes. However, an unusual feature of that $Ti_3C_2T_z$ clay (Figure 2) is the presence of crystalline structures intercalating the layers. Based on the EDS data shown in Figure S2, the crystalline structures are likely SnF_2 and AlF_3. We hypothesize that the SnF_2 diffused in between the layers during etching, and AlF_3 formed between the layers. The large spheres that are present are made of Sn that agglomerates, as F is consumed from SnF_2 is used up during the etching. The EDS mapping and chemical composition of $Ti_3C_2T_z$ clay is shown in Figure S2 and Table S1, confirming successful removal of the A-layer form the parent MAX phase.

Without the KOH wash step, we could not produce a stable $Ti_3C_2T_z$ nanosheet dispersion; we hypothesized that the colloidal instability is likely due to a lack of -OH terminal groups, which are present on $Ti_3C_2T_z$ nanosheet synthesized by conventional HF etching technique. With this in mind, the $Ti_3C_2T_z$ clay was

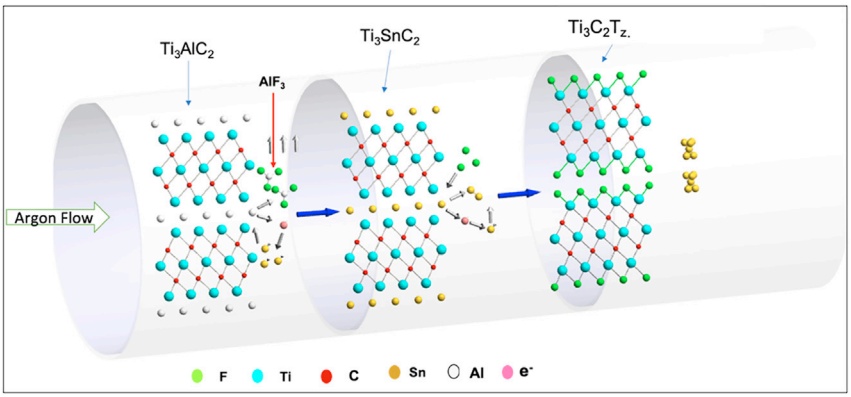

Figure 1. Schematic of the reaction setup used for molten salt etching in a tube furnace under argon flow to minimize the interference of oxygen during etching

washed with 0.1M KOH solution for 2 h to add these -OH terminal groups and allow for dispersibility. In addition, the KOH wash also dissolves and remove the excess SnF_2 entrapped inside the $Ti_3C_2T_z$ clay (Figure S2). The EDS mapping and chemical composition of $Ti_3C_2T_z$ clay before and after KOH washing is shown in Figure S2 and Table S1, which confirms the removal of unreacted or excess SnF_2 based on the decrease in fluorine content.

KOH-washed $Ti_3C_2T_z$ clay was then intercalated with DMSO for 20 h and washed with water 3–4 times to remove DMSO. After intercalation, the $Ti_3C_2T_z$ clay was delaminated by bath sonication for 1 h. The resulting mixture was then centrifuged. This results in the formation of stable dispersion of $Ti_3C_2T_z$ nanosheets (Figure 2D) in the supernatant (Figure S3). The supernatant contained some Sn spheres along with the $Ti_3C_2T_z$ nanosheets; in order to remove these impurities, a two-stage centrifuge method was used (Figure S4). The two-stage centrifuge method consists of a light centrifuging at 5,000 rpm for 10 min and an additional heavy centrifuging of the supernatant at 9,000 rpm for 20 min. The additional images (Figure S5) of $Ti_3C_2T_z$ MXene nanosheets confirm the formation of single-layer nanosheets. The resulting $Ti_3C_2T_z$ nanosheets are colloidally stable with a negative ζ potential of −31.7 mV (Figure 3) and 359 nm particle size (measured by DLS). A typical AFM image of the $Ti_3C_2T_z$ nanosheets is presented in Figure S6 showing typical nanosheet thicknesses of 1.5–2.5 n.

The SEM and EDS mapping (Figure 4) indicate an elemental composition (Table 1) for exfoliated $Ti_3C_2T_z$ and delaminated $Ti_3C_2T_z$ nanosheets of Ti/F/C = 29.7:18.1:14.6 (wt. %) and Ti/F/C = 29.1:20.7:17.7 (wt. %), respectively. Element mappings reveal that Ti, C, O, and F atoms are uniformly distributed throughout the entire structure (Figure 4), where F and O atoms are from the introduced -F, -OH, and -O group. These functional groups are important for achieving high capacitance in aqueous electrolytes. Also, the reduction in the amount of Al compared with the parent MAX (Table S1) indicates the selective etching of Al. Based on the aluminum removed (measured by EDS), the $Ti_3C_2T_z$ MXene clay yield was found to be ~82%. Based on the $Ti_3C_2T_z$ MXene nanosheet mass in the final product, we got a nanosheet yield of 10%.

The MXene sample surface was further analyzed by X-ray photoelectron spectroscopy (XPS). The XPS survey spectrum (Figure 5A) of the MXene nanosheets powder showed the presence of C, Ti, O, Sn, and F elements. High-resolution spectra for the Ti 2p, C 1s and Sn 3d binding energies are shown in Figures 5B–5D, respectively. The high-resolution XPS spectra of Ti 2p (Figure 5B) region were deconvoluted into Ti–C, Ti^{2+}, Ti^{3+}, TI-F, and TiO_2, which matches with prior studies (Halim et al., 2016; Magnuson et al., 2018; Natu et al., 2021; Naguib et al., 2011). The presence of the Ti-C peak at binding energy of 455 eV in Ti 2p spectra indicates the removal of aluminum from MAX phase and formation of $Ti_3C_2T_z$ MXene nanosheets. The Ti signals of various oxidation states is a result of nonuniform surface terminations ($Ti_3C_2F_z$/$Ti_3C_2(OH)_z$) (Satheeshkumar et al., 2016). In addition, the peak at 281.9 eV also confirms the presence of C-Ti-(OH/F), which is in agreement with previous research done by Naguib et al. (Naguib et al., 2011). The high-resolution spectra of C 1s region (Figure 5C) of the powder show three prominent peaks at 282, 284.6, and 286.6 eV, which corresponds to Ti-C, C-C, and C-O, respectively (Halim et al., 2016; Naguib et al., 2011; Natu et al., 2021). The presence of Ti-C peak in C 1s spectra confirms the formation of MXene (Ghidiu et al.,

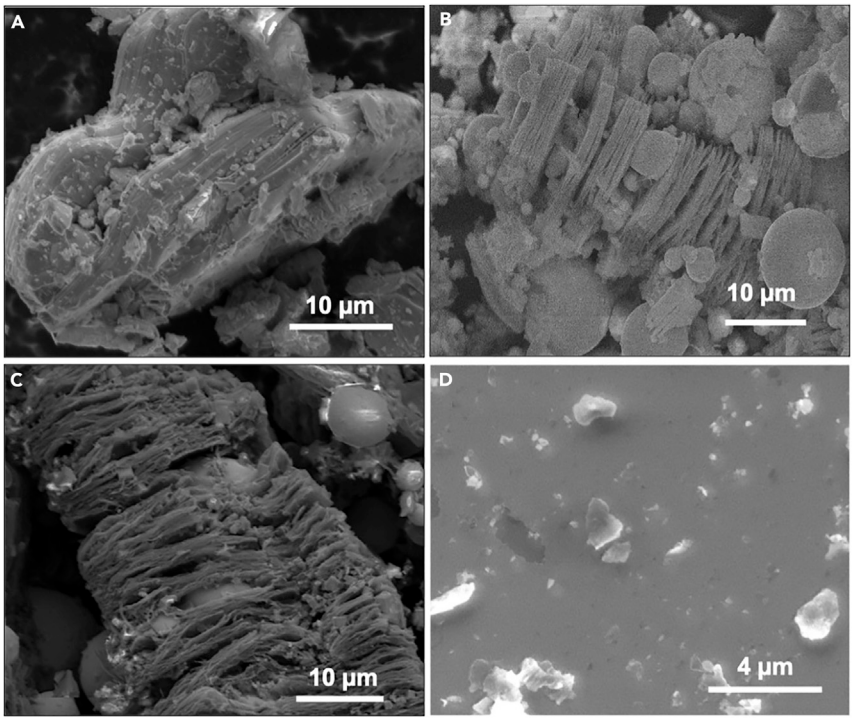

Figure 2. SEM of MXene at each step
(A) Parent Ti_3AlC_2 MAX phase.
(B) $Ti_3C_2T_z$ before KOH wash (freeze dried).
(C) $Ti_3C_2T_z$ after KOH wash (freeze dried).
(D) $Ti_3C_2T_z$ nanosheets drop-cast from aqueous dispersion.

2014b; Halim et al., 2016; Naguib et al., 2011). The only unusual feature observed in the XPS spectra is the presence of Sn, which corresponds to unreacted salt that was not removed during the KOH and water washings. The peaks in Sn 3d spectra (Figure 5D) at 487 eV and 495.5 eV correspond to Sn $3d_{5/2}$ and Sn $3d_{3/2}$, respectively (Pan et al., 2012; Zatsepin et al., 2016). The fitted curves correspond to different oxidation states of Sn (Sn, Sn^{2+}, and Sn^{4+}).

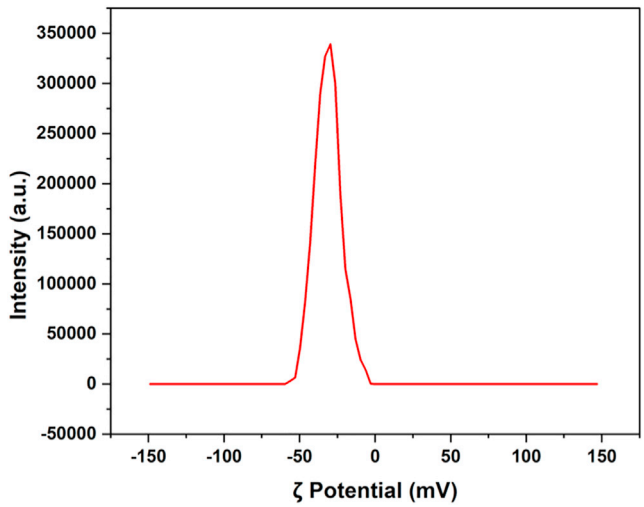

Figure 3. ζ potential of delaminated $Ti_3C_2T_z$ nanosheets indicating the colloidal stability of aqueous dispersion of nanosheets

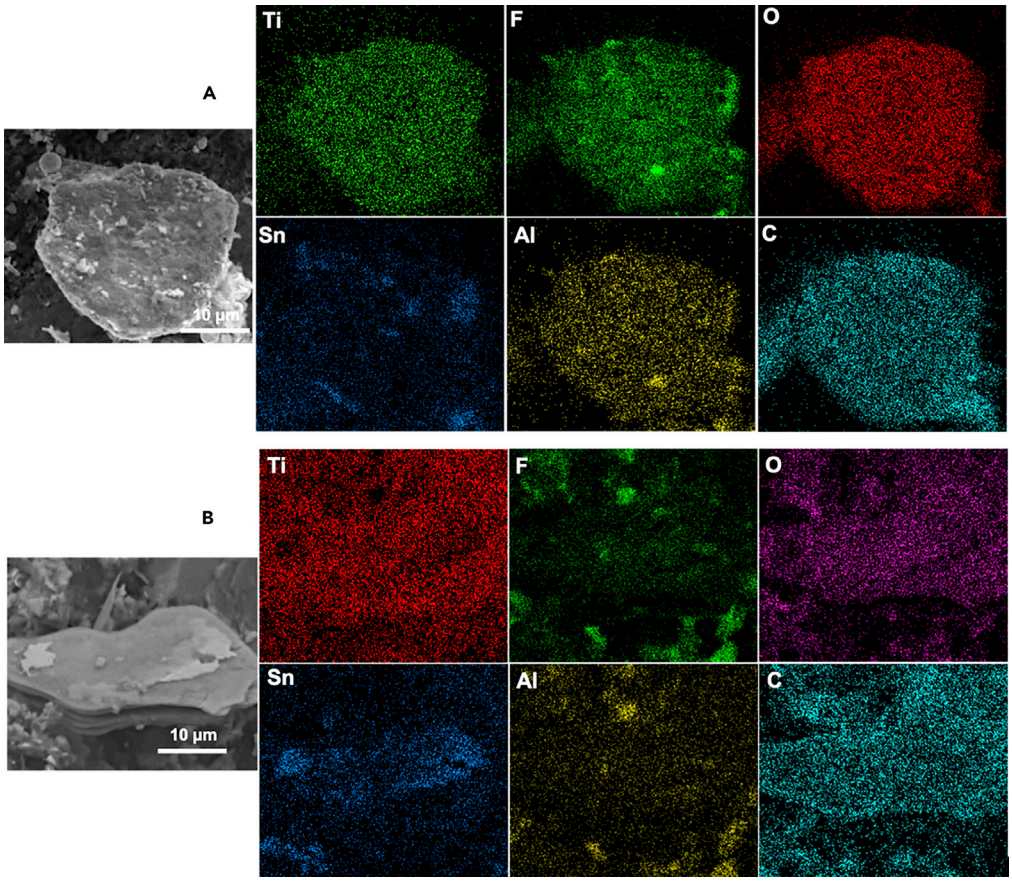

Figure 4. EDS of MXene

(A) Delaminated $Ti_3C_2T_z$ nanosheets.

(B) Exfoliated $Ti_3C_2T_z$; we can clearly see the lower %wt. of Al, which indicates successful etching of Al from Ti_3AlC_2.

Transmission electron microscopy (TEM) was used to determine the morphology of $Ti_3C_2T_z$ nanosheets. The TEM (Figure 6A) demonstrates the typical $Ti_3C_2T_z$ nanosheet morphology. The TEM image shows low contrast between the nanosheet and the background, indicating that this nanosheet is single to few layers in thickness. The UV-Vis spectra of the supernatant product are quite similar to that of conventional acid-etched MXene products (Figure S7).

To investigate the formation of $Ti_3C_2T_z$, we further performed X-ray diffraction (XRD); Figure 6B shows the XRD patterns of $Ti_3C_2T_z$ clay before and after the KOH wash, along with the XRD of $Ti_3C_2T_z$ nanosheets from

Table 1. Elemental composition of exfoliated and delaminated $Ti_3C_2T_z$ nanosheets obtained from EDS analysis corresponding to Figure 4

$Ti_3C_2T_z$	Exfoliated nanosheet	Delaminated nanosheet
Element	% Weight	% Weight
Ti	29.7	29.1
Sn	19	9.3
F	18.1	20.7
O	15	21.6
C	14.6	17.7
Al	3.5	1.6

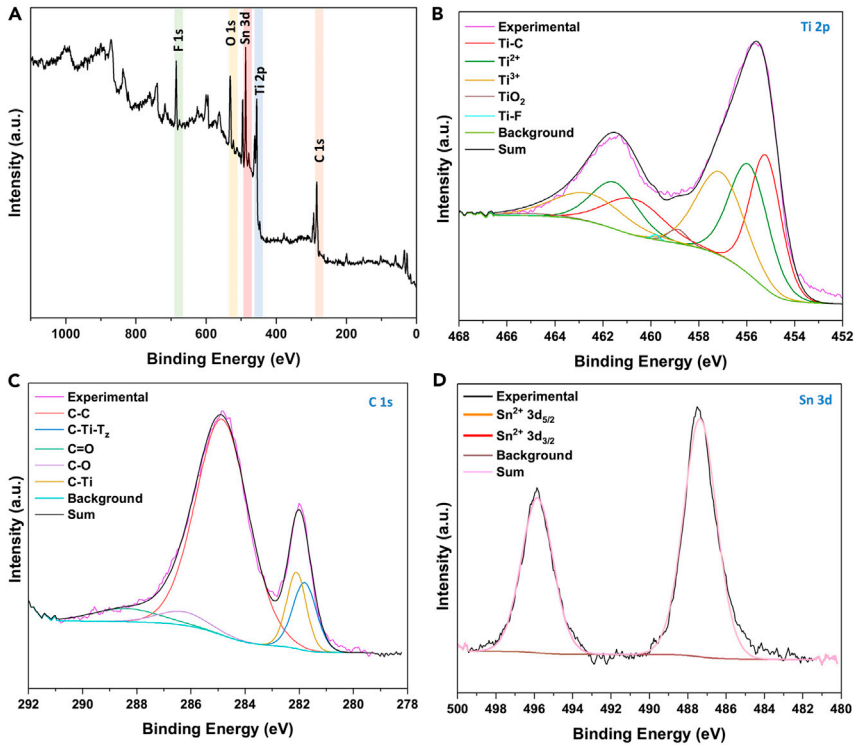

Figure 5. Deconvoluted XPS spectra of $Ti_3C_2T_z$ nanosheets

(A and B) (A) Survey; high-resolution spectra of (B) Ti 2p.

(C) C 1s.

(D) Sn 3d.

the supernatant. The nonbasal plane peaks of Ti_3AlC_2 were not seen in the XRD, which indicates the successful etching of Al from Ti_3AlC_2. The characteristic peaks of $Ti_3C_2T_z$ are found at 9.4° and 19°, which confirms the formation of $Ti_3C_2T_z$ (Iqbal et al., 2019). The $Ti_3C_2T_z$ peak observed in the case of molten salt etching matches with the traditionally HF-etched $Ti_3C_2T_z$. Also, there is a possibility that the nanosheets are unable to align in close proximity to each other due to the presence of Sn (small amount). The large peaks from 30°, 33°, 44°, and 45° are characteristic of Sn, which is a byproduct of the etching process described in the reaction mechanism (Data S1).

We further support our finding of $Ti_3C_2T_z$ MXene formation by measuring the Raman spectra of the nanosheet powder (Figure 6C). The prominent peaks for $Ti_3C_2T_z$ MXene in Figure 6C at 384 cm^{-1} and 622 cm^{-1} correspond to the nonstoichiometric Ti–C and C–C vibrations (Cao et al., 2017; Elumalai et al., 2020; Dong et al., 2017; Ding et al., 2019; Lorencova et al., 2017; Naguib et al., 2014a). Another two bands were detected at around 1,352 cm^{-1} (D band) and 1,558 cm^{-1} (G band), and these two broad peaks of D and G bands are associated with the carbon-carbon vibrations (Saha et al., 2021a; Zhao et al., 2016). The G-band peak is associated with the stretching of the C-C bond in carbon materials, and this is observed in all sp^2 carbon systems (Saha et al., 2021b). The D band corresponds to scattering from defects or disorder of carbon (Cao et al., 2017; Ding et al., 2019). The ratio of D and G band intensities was observed to be nearly 1.

The produced nanosheets are electrically conductive; the vacuum-filtered film showed a conductivity of 706 S/m. The different functional group distribution than the acid-etched MXene might be the reason behind the different conductivity performance. We also confirmed these conductive nanosheet films' ability to heat in response to radio frequency fields, similar to our prior paper (Figure S8) (Habib et al., 2019).

CONCLUSIONS

In conclusion, an alternative approach of molten salt etching is proposed as an alternative to the traditional HF etching. The new approach resulted in successful synthesis of water dispersible $Ti_3C_2T_z$. This new

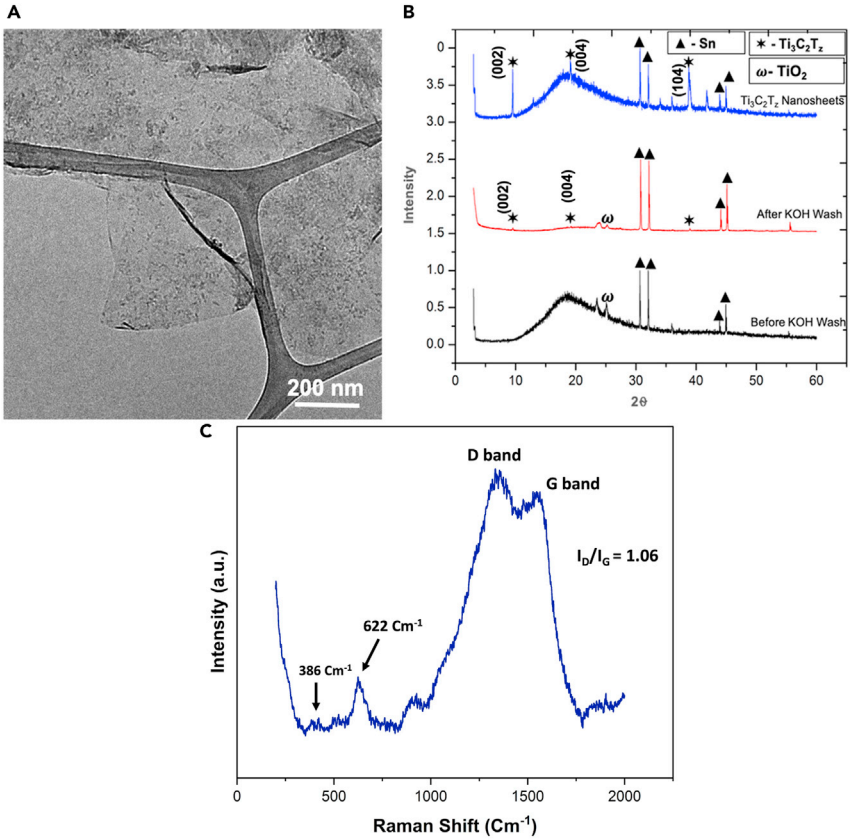

Figure 6. Characterization of $Ti_3C_2T_z$ nanosheets

(A) TEM of $Ti_3C_2T_z$ nanosheet (supernatant).

(B) XRD of $Ti_3C_2T_z$ clay before KOH washing, after KOH washing, and $Ti_3C_2T_z$ nanosheet (final supernatant).

(C) The Raman spectra of $Ti_3C_2T_z$ MXene nanosheet powder.

approach will open up the new avenues for safer scales of $Ti_3C_2T_z$ production on a commercial level without the use of hazardous HF or other acids. The SEM, TEM, EDS, and XRD confirm the formation of $Ti_3C_2T_z$ nanosheets by etching in the molten SnF_2 salt. However, the separation process is crucial to separate the $Ti_3C_2T_z$ nanosheets from the mixture of MAX phase spheres. These exciting findings open up a new, safe, industrially viable method to make dispersible $Ti_3C_2T_z$ nanosheets.

Limitations of the study

The key limitation of this work is the presence of Sn or SnF_2 in the MXene nanosheets and the difficulties associated with removing the Sn entirely.

STAR★METHODS

Detailed methods are provided in the online version of this paper and include the following:

- KEY RESOURCES TABLE
- RESOURCE AVAILABILITY
  - Lead contact
  - Materials availability
  - Data and code availability
- EXPERIMENTAL MODEL AND SUBJECT DETAILS
  - Synthesis of Ti_3AlC_2 MAX phase
  - Synthesis of $Ti_3C_2T_z$
- METHOD DETAILS
  - Materials

- Synthesis
- Sample preparation
- QUANTIFICATION AND STATISTICAL ANALYSIS
  - Scanning electron microscopy (SEM)
  - X-Ray diffraction (XRD)
  - Energy dispersive spectroscopy (EDS)
  - Transmission electron microscopy (TEM)
  - Atomic force microscopy (AFM)
  - UV-vis spectroscopy
  - Radio frequency (RF) heating
  - Dynamic light scattering (DLS)
  - ζ potential measurement
  - X-Ray photoelectron spectroscopy (XPS)
  - Raman spectroscopy

SUPPLEMENTAL INFORMATION

Supplemental information can be found online at https://doi.org/10.1016/j.isci.2021.103403.

ACKNOWLEDGMENTS

This work is funded by National Science Foundation (Grant CMMI-1760859). We would like to acknowledge the use of the TAMU Materials Characterization Facility and TAMU Microscopy & Imaging Center. We would also like to acknowledge Dr Mustafa Akbulut and his student Shuhao Liu of TAMU for allowing us to use his group's ZetaSizer instrument for zeta potential and dynamic light scattering measurements.

AUTHOR CONTRIBUTIONS

K.A., J.B., and M.G. conceived and designed the project. K.A., J.B., S.S., D.H., X.Z., A.S., and H.C. performed the experiments, characterization, and analysis, with input from J.L., M.R., and M.G. Finally, K.A., J.B., M.R., and M.G. wrote the manuscript with consultation from all authors. M.G. supervised the project.

DECLARATION OF INTERESTS

The authors declare no competing interests.

Received: July 26, 2021
Revised: September 29, 2021
Accepted: November 3, 2021
Published: December 17, 2021

REFERENCES

Barsoum, M.W. (2000). The MN+ 1AXN phases: a new class of solids: thermodynamically stable nanolaminates. Prog. Solid State Chem. *28*, 201–281.

Cao, H., Escamilla, M., Arole, K.D., Holta, D., Lutkenhaus, J.L., Radovic, M., Green, M.J., and Pentzer, E.B. (2021). Flocculation of MXenes and their use as 2D particle surfactants for capsule formation. Langmuir *37*, 2649–2657.

Cao, M., Wang, F., Wang, L., Wu, W., Lv, W., and Zhu, J. (2017). Room temperature oxidation of Ti3C2 MXene for supercapacitor electrodes. J. Electrochem. Soc. *164*, A3933.

Ding, G., Zeng, K., Zhou, K., Li, Z., Zhou, Y., Zhai, Y., Zhou, L., Chen, X., and Han, S.-T. (2019). Configurable multi-state non-volatile memory behaviors in Ti 3 C 2 nanosheets. Nanoscale *11*, 7102–7110.

Dong, Y., Wu, Z.-S., Zheng, S., Wang, X., Qin, J., Wang, S., Shi, X., and Bao, X. (2017). Ti3C2 MXene-derived sodium/potassium titanate nanoribbons for high-performance sodium/potassium ion batteries with enhanced capacities. ACS Nano *11*, 4792–4800.

Eklund, P., Beckers, M., Jansson, U., Högberg, H., and Hultman, L. (2010). The Mn+ 1AXn phases: materials science and thin-film processing. Thin Solid Films *518*, 1851–1878.

Eklund, P., Rosen, J., and Persson, P.O.Å. (2017). Layered ternary M n+ 1AX n phases and their 2D derivative MXene: an overview from a thin-film perspective. J. Phys. D Appl. Phys. *50*, 113001.

Elumalai, S., Lombardi, J.R., and Yoshimura, M. (2020). The surface-enhanced resonance Raman scattering of dye molecules adsorbed on two-dimensional titanium carbide Ti 3 C 2 T x (MXene) film. Mater. Adv. *1*, 146–152.

Feng, A., Yu, Y., Jiang, F., Wang, Y., Mi, L., Yu, Y., and Song, L. (2017). Fabrication and thermal stability of NH4HF2-etched Ti3C2 MXene. Ceramics Int. *43*, 6322–6328.

Ghidiu, M., Lukatskaya, M.R., Zhao, M.-Q., Gogotsi, Y., and Barsoum, M.W. (2014a). Conductive two-dimensional titanium carbide 'clay'with high volumetric capacitance. Nature *516*, 78–81.

Ghidiu, M., Naguib, M., Shi, C., Mashtalir, O., Pan, L., Zhang, B., Yang, J., Gogotsi, Y., Billinge, S.J., and Barsoum, M.W. (2014b). Synthesis and characterization of two-dimensional Nb 4 C 3 (MXene). Chem. Commun. *50*, 9517–9520.

Habib, T., Patil, N., Zhao, X., Prehn, E., Anas, M., Lutkenhaus, J.L., Radovic, M., and Green, M.J. (2019). Heating of Ti 3 C 2 T x MXene/polymer composites in response to Radio Frequency fields. Sci. Rep. *9*, 1–7.

Halim, J., Cook, K.M., Naguib, M., Eklund, P., Gogotsi, Y., Rosen, J., and Barsoum, M.W. (2016). X-ray photoelectron spectroscopy of select multi-layered transition metal carbides (MXenes). Appl. Surf. Sci. *362*, 406–417.

Iqbal, M.A., Tariq, A., Zaheer, A., Gul, S., Ali, S.I., Iqbal, M.Z., Akinwande, D., and Rizwan, S. (2019). Ti3C2-MXene/Bismuth ferrite nanohybrids for efficient degradation of organic dyes and colorless pollutants. ACS Omega *4*, 20530–20539.

Kamysbayev, V., Filatov, A.S., Hu, H., Rui, X., Lagunas, F., Wang, D., Klie, R.F., and Talapin, D.V. (2020). Covalent surface modifications and superconductivity of two-dimensional metal carbide MXenes. Science *369*, 979–983.

Khazaei, M., Ranjbar, A., Arai, M., Sasaki, T., and Yunoki, S. (2017). Electronic properties and applications of MXenes: a theoretical review. J. Mater. Chem. C *5*, 2488–2503.

Kim, S.J., Koh, H.-J., Ren, C.E., Kwon, O., Maleski, K., Cho, S.-Y., Anasori, B., Kim, C.-K., Choi, Y.-K., and Kim, J. (2018). Metallic Ti3C2T x MXene gas sensors with ultrahigh signal-to-noise ratio. ACS Nano *12*, 986–993.

Lakhe, P., Prehn, E.M., Habib, T., Lutkenhaus, J.L., Radovic, M., Mannan, M.S., and Green, M.J. (2019). Process safety analysis for Ti3C2T x MXene synthesis and processing. Ind. Eng. Chem. Res. *58*, 1570–1579.

Li, M., Han, M., Zhou, J., Deng, Q., Zhou, X., Xue, J., Du, S., Yin, X., and Huang, Q. (2018). Novel scale-like structures of graphite/TiC/Ti3C2 hybrids for electromagnetic absorption. Adv. Electron. Mater. *4*, 1700617.

Li, M., Lu, J., Luo, K., Li, Y., Chang, K., Chen, K., Zhou, J., Rosen, J., Hultman, L., and Eklund, P. (2019). Element replacement approach by reaction with Lewis acidic molten salts to synthesize nanolaminated MAX phases and MXenes. J. Am. Chem. Soc. *141*, 4730–4737.

Li, Y., Shao, H., Lin, Z., Lu, J., Liu, L., Duployer, B., Persson, P.O., Eklund, P., Hultman, L., and Li, M. (2020). A general Lewis acidic etching route for preparing MXenes with enhanced electrochemical performance in non-aqueous electrolyte. Nat. Mater. *19*, 894–899.

Lorencova, L., Bertok, T., Dosekova, E., Holazova, A., Paprckova, D., Vikartovska, A., Sasinkova, V., Filip, J., Kasak, P., and Jerigova, M. (2017). Electrochemical performance of Ti3C2Tx MXene in aqueous media: towards ultrasensitive H2O2 sensing. Electrochim. Acta *235*, 471–479.

Magnuson, M., Halim, J., and Näslund, L.-Å. (2018). Chemical bonding in carbide MXene nanosheets. J. Electron Spectrosc. Relat. Phenomena *224*, 27–32.

Naguib, M., Kurtoglu, M., Presser, V., Lu, J., Niu, J., Heon, M., Hultman, L., Gogotsi, Y., and Barsoum, M.W. (2011). Two-dimensional nanocrystals produced by exfoliation of Ti3AlC2. Adv. Mater. *23*, 4248–4253.

Naguib, M., Mashtalir, O., Carle, J., Presser, V., Lu, J., Hultman, L., Gogotsi, Y., and Barsoum, M.W. (2012). Two-dimensional transition metal carbides. ACS Nano *6*, 1322–1331.

Naguib, M., Mashtalir, O., Lukatskaya, M.R., Dyatkin, B., Zhang, C., Presser, V., Gogotsi, Y., and Barsoum, M.W. (2014a). One-step synthesis of nanocrystalline transition metal oxides on thin sheets of disordered graphitic carbon by oxidation of MXenes. Chem. Commun. *50*, 7420–7423.

Naguib, M., Mochalin, V.N., Barsoum, M.W., and Gogotsi, Y. (2014b). 25th anniversary article: MXenes: a new family of two-dimensional materials. Adv. Mater. *26*, 992–1005.

Natu, V., Benchakar, M., Canaff, C., Habrioux, A., Celerier, S., and Barsoum, M.W. (2021). A critical analysis of the X-ray photoelectron spectra of Ti3C2Tz MXenes. Matter.

Pan, S., Wang, S., Zhang, Y., Luo, Y., Kong, F., Xu, S., Xu, J., and Li, G. (2012). P-type conduction in nitrogen-doped SnO 2 films grown by thermal processing of tin nitride films. Appl. Phys. A *109*, 267–271.

Persson, I., Halim, J., Lind, H., Hansen, T.W., Wagner, J.B., Näslund, L.Å., Darakchieva, V., Palisaitis, J., Rosen, J., and Persson, P.O. (2019). 2D transition metal carbides (MXenes) for carbon capture. Adv. Mater. *31*, 1805472.

Ran, J., Gao, G., Li, F., Ma, T., Du, A., and Qiao, S. (2017). Ti_3C_2 mxene co-catalyst on metal sulfide photo-absorbers for enhanced visible-light photocatalytic hydrogen production. Nat. Commun. *8*, 13907.

Saha, S., Arole, K., Radovic, M., Lutkenhaus, J., and Green, M. (2021a). One-step hydrothermal synthesis of porous Ti3C2Tz MXene/rGO gels for supercapacitor applications. Nanoscale *13*, 16543–16553.

Saha, S., Lakhe, P., Mason, M.J., Coleman, B.J., Arole, K., Zhao, X., Yakovlev, S., Uppili, S., Green, M.J., and Hule, R.A. (2021b). Sustainable production of graphene from petroleum coke using electrochemical exfoliation. NPJ 2D Mater. Appl. *5*, 1–8.

Satheeshkumar, E., Makaryan, T., Melikyan, A., Minassian, H., Gogotsi, Y., and Yoshimura, M. (2016). One-step solution processing of Ag, Au and Pd@ MXene hybrids for SERS. Sci. Rep. *6*, 1–9.

Seh, Z.W., Fredrickson, K.D., Anasori, B., Kibsgaard, J., Strickler, A.L., Lukatskaya, M.R., Gogotsi, Y., Jaramillo, T.F., and Vojvodic, A. (2016). Two-dimensional molybdenum carbide (MXene) as an efficient electrocatalyst for hydrogen evolution. ACS Energy Lett. *1*, 589–594.

Shah, S., Habib, T., Gao, H., Gao, P., Sun, W., Green, M., and Radovic, M. (2017). Template-free 3D titanium carbide (Ti 3 C 2 T x) MXene particles crumpled by capillary forces. Chem. Commun. *53*, 400–403.

Shahzad, F., Alhabeb, M., Hatter, C.B., Anasori, B., Hong, S.M., Koo, C.M., and Gogotsi, Y. (2016). Electromagnetic interference shielding with 2D transition metal carbides (MXenes). Science *353*, 1137–1140.

Tang, Q., Zhou, Z., and Shen, P. (2012). Are MXenes promising anode materials for Li ion batteries? Computational studies on electronic properties and Li storage capability of Ti3C2 and Ti3C2X2 (X= F, OH) monolayer. J. Am. Chem. Soc. *134*, 16909–16916.

Tezel, G.B., Arole, K., Holta, D.E., Radovic, M., and Green, M.J. (2022). Interparticle interactions and rheological signatures of Ti3C2Tz MXene dispersions. J. Colloid Interf. Sci. *605*, 120–128.

Urbankowski, P., Anasori, B., Makaryan, T., Er, D., Kota, S., Walsh, P.L., Zhao, M., Shenoy, V.B., Barsoum, M.W., and Gogotsi, Y. (2016). Synthesis of two-dimensional titanium nitride Ti 4 N 3 (MXene). Nanoscale *8*, 11385–11391.

Zatsepin, D., Zatsepin, A., Boukhvalov, D., Kurmaev, E., and Gavrilov, N. (2016). Sn-loss effect in a Sn-implanted a-SiO2 host-matrix after thermal annealing: a combined XPS, PL, and DFT study. Appl. Surf. Sci. *367*, 320–326.

Zhao, C., Wang, Q., Zhang, H., Passerini, S., and Qian, X. (2016). Two-dimensional titanium carbide/RGO composite for high-performance supercapacitors. ACS Appl. Mater. Inter. *8*, 15661–15667.

STAR★METHODS

KEY RESOURCES TABLE

REAGENT or RESOURCE	SOURCE	IDENTIFIER
Chemicals, peptides, and recombinant proteins		
Ti elemental powder (325 mesh, 99%)	Alfa Aesar	CAS Number 7440-32-6
Al elemental powder (325 mesh, 99.5%),	Alfa Aesar	CAS Number 7429-90-5
Graphite (10 micron, 99%).	Alfa Aesar	CAS Number 7782-42-5
SnF_2 (99%)	Acros Organics	CAS Number 7783-47-3
KOH	Sigma Aldrich	CAS Number 1310-58-3
DMSO	Sigma Aldrich	CAS Number 67-68-5
Software and algorithms		
OriginLab	OriginLab Corporation	https://www.originlab.com/

RESOURCE AVAILABILITY

Lead contact

Further information and requests for resources and reagents should be directed to the lead contact, Micah Green (micah.green@tamu.edu)

Materials availability

This study did not generate new unique reagents.

Data and code availability

Data reported in this paper will be shared by the lead contact upon request. No new code was generated during this study.

EXPERIMENTAL MODEL AND SUBJECT DETAILS

Synthesis of Ti_3AlC_2 MAX phase

Pressureless reaction sintering was used to synthesize parent MAX phases for etching. For Ti_3AlC_2, elemental powers powders of titanium, aluminum, and graphite were scaled in the molar ratio of 3:1.2:1.95, respectively. The powders were milled in a jar rolling mill with 35 mm high-density ZrO_2 cylinders at 300 RPM for 12 h to prepare a homogeneous mixture. After mixing, the elemental powders were loaded into alumina crucibles, which were inserted into diameter alumina tube vacuum furnace (MTI Corporation, GSL-1600X-50-UL). Once sealed, a vacuum was pulled on the tube to an ultimate pressure of 10^{-3} torr, followed by a short purge with ultra-high purity argon (UHP Ar). This step was repeated three times to ensure the removal of air. While maintaining a constant flow of UHP Ar, the samples were heated at a rate of 10°C/min to 1510°C and dwelled for 4 h. After dwelling, the samples cooled naturally. The resulting bulk MAX phase was crushed using an alumina mortar and pestle and were sieved through a 325-mesh sieve to obtain powders of a suitable size for etching.

Synthesis of $Ti_3C_2T_z$

The $Ti_3C_2T_z$ was prepared by a reaction between the MAX phase precursor (Ti_3AlC_2) and SnF_2. For synthesizing $Ti_3C_2T_z$, a mixture of powder with a molar ratio of Ti_3AlC_2/SnF_2 = 1:6 was used as a starting reaction material. The starting material was mixed thoroughly by stirring with a glass rod. Then, the mixture powder was transferred into an alumina boat. The alumina boat was loaded into a tube furnace (Thermo Scientific Lindberg/Blue M TF55030A) and heated for 6 h at 550°C under flowing UHP Ar. After the reaction, the product was washed with 0.1M potassium hydroxide (KOH) to dissolve the excess salt and subsequently washed with deionized water 4 times to remove the residual KOH. The $Ti_3C_2T_z$ clay was then redispersed into DMSO for intercalation for 20 h, and then washed with water 3–4 times to remove DMSO. Sediment was then redispersed in water and bath sonicated for 60 min to delaminate the nanosheets. Finally, the bath

sonicated dispersion is centrifuged for 20 min on 3500 RPM. $Ti_3C_2T_z$ nanosheets obtained in the supernatant were freeze-dried for further characterization.

METHOD DETAILS

Materials

The elemental powders used to prepare parent MAX phases were titanium (Alfa Aesar, −325 mesh, 99%), aluminum (Alfa Aesar, −325 mesh, 99.5%), and graphite (Alfa Aesar, 7–10 micron, 99%). The bucky paper used were supplied by Pall Laboratory. Tin fluoride (SnF2) used were supplied by Acros Organics. The Potassium Hydroxide (KOH) pellets and Dimethyl Sulfoxide (DMSO) were ordered from Sigma Aldrich.

Synthesis

The synthesis procedure for the Ti_3AlC_2 MAX phase and $Ti_3C_2T_z$ MXene is explained in detail under the section "experimental model and subject details".

Sample preparation

The details about the sample preparation for various characterization techniques are listed under the section "quantification and statistical analysis".

QUANTIFICATION AND STATISTICAL ANALYSIS

Scanning electron microscopy (SEM)

The morphologies of $Ti_3C_2T_z$ clay and nanosheets were observed with a FEI Quanta 600 field-emission scanning electron microscope. For imaging, the vigorously mixed dispersions of MXenes were freeze-dried for 24 h. The acceleration voltage used in the imaging was 5 kV. The SEM samples were prepared by drop-casting the diluted dispersion of $Ti_3C_2T_z$ on a silicon wafer and letting it dry in a vacuum overnight.

X-Ray diffraction (XRD)

XRD patterns of dried $Ti_3C_2T_z$ were obtained using Bruker D8 powder X-ray diffractometer fitted with LynxEye detector, in a Bragg Brentano geometry with CuKa (l = 1.5418 A) radiation source. The XRD was performed with a step size of 0.02° and a scan rate of 1.5 s per step. The $Ti_3C_2T_z$ samples were freeze-dried before the XRD. A zero-background sample holder was used in all the tests.

Energy dispersive spectroscopy (EDS)

Elemental composition analysis was done using an Oxford EDS detector on FEI Quanta 600 SEM, and results were analyzed using AZtec software by Oxford Instruments. The powdered sample was exposed to a beam, and imaging was done at 20 kV acceleration voltage.

Transmission electron microscopy (TEM)

3 mL of $Ti_3C_2T_z$ dispersion in water was drop cast on a holey carbon grid, and the grid was pre-treated by glow-discharging to make it hydrophilic. The excess solution was wiped off with a filter paper and then air-dried. The samples were imaged by using an FEI Tecnai F20 transmission electron microscope operating at 200 kV.

Atomic force microscopy (AFM)

$Ti_3C_2T_z$ dispersion was again diluted with water and drop-cast on a freshly cleaved mica substrate. The mica substrate was allowed to dry overnight in a vacuum oven at 30°C. The samples were imaged using Bruker Dimension Icon AFM for scanning probe microscopy, and height profiles were obtained with a MultiMode™ scanning probe microscope.

UV-vis spectroscopy

UV–Vis measurements were done using Shimadzu UV−vis 2550. The sample used for UV Vis absorption spectra was $Ti_3C_2T_z$ dispersion in water with a 0.4 mg/mL concentration. The readings were taken multiple times to achieve maximum accuracy.

Radio frequency (RF) heating

A stationary, fringing field applicator fabricated in –house by laser-etching copper traces on an FR4 substrate was used for this experiment. The copper traces with spacing 4 mm act as capacitors, resulting in a fringing field coming out-of-the-plane of the applicator. The RF field was generated using a RIGOL DSG815 signal generator, which were then amplified using a PRANA GN 500 amplifier and supplied to the applicator via a coaxial cable. The frequency was hand-tuned to obtain maximum heating rate, and temperature vs. time was observed at that frequency for powers 1 and 10 W. The sample used for the RF study was a buckypaper, which was made by vacuum filtration of MXene dispersion using Supor Polyethersulfone Membrane (Pall Laboratory).

Dynamic light scattering (DLS)

The hydrodynamic diameters of aqueous $Ti_3C_2T_z$ nanosheets were determined at ambient temperature by DLS at a scattering angle of 90° using a Zetasizer Nano ZS90 from Malvern Instruments. The colloidal aqueous dispersion of $Ti_3C_2T_z$ nanosheets was diluted to a concentration of around 0.009 mg/mL before making the measurements.

ζ potential measurement

ζ potential of $Ti_3C_2T_z$ nanosheets in water were measured at ambient temperature using the Zetasizer Nano ZS90 from Malvern Instruments and the appropriate capillary cell, DTS 1070, from Malvern Instruments. The $Ti_3C_2T_z$ nanosheets dispersion was diluted to a concentration around 0.009 mg/mL before measurements to ensure consistency. Each test was repeated 2 times, and an averaged value was derived to ensure accuracy.

X-Ray photoelectron spectroscopy (XPS)

XPS was performed using an Omicron X-ray photoelectron spectrometer employing a Mg-sourced X-ray beam at 15 kV with an aperture of 5.

Raman spectroscopy

Raman spectra were measured using Horiba Jobin-Yvon LabRam HR with laser wavelength of 633 nm, laser power of 1.91 mW, exposure time of 10 s, and four accumulations. The "Auto" baseline correction method in LabSpec was used to remove baseline.